

Large-scale mean flow and inclination of isolated turbulent band in channel flow

Linsen Zhang and Jianjun Tao*

CAPT-HEDPS, SKLTCS, Department of Mechanics and Engineering Science,
College of Engineering, Peking University, Beijing 100871, China

(Dated: October 6, 2023)

Isolated turbulent bands observed in transitional channel flows have downstream heads and inclined bulks at a characteristic angle. In the large-scale mean flow, a ν -shape vortex found at the head elongates into the bulk part, forming a pair of counter-rotating vortex tube structures. It is revealed numerically and theoretically that the head and the bulk convection velocities reflect the obliquely forward and the backward self-induced velocities of the ν -shape vortex and the vortex tube pair, respectively, and the difference between these convection velocities provides a restoring angular momentum to retain the characteristic inclination angle through a self-adjustment process.

Formation of localized turbulence in wall-bounded shear flows is one of the least understood phenomena in fluid dynamics [1–3]. As the precursor of the laminar-turbulent transition in plane-Poiseuille flow (pPF), isolated turbulent band (ITB) triggered by localized perturbations has been observed numerically [4–9] and experimentally [10–12], and illustrates fascinating features, e.g., its bulk part extends obliquely with a characteristic inclination angle. The oblique growth of turbulent patches is found to be related to the mismatch of streamwise flow rates [13], and suitably tilted computational domains are used to simulate the transitional flows [14, 15]. For plane-Couette flow (pCF), invariant solutions [16] bifurcated from the Nagata equilibrium [17] are found to retain for a limited range of pattern angles [18], while the nonlinear traveling wave solutions obtained for pPF exist in a wide range of oblique angles [11]. When the Reynolds number decreases from a high value, alternating laminar and turbulent stripes or bands emerge from featureless turbulence in pCF [19, 20] and pPF [21], but these periodic oblique bands are different from the ITB, which has an energetic downstream end or ITB head and a decaying upstream tail, and is surrounded by a large area of laminar flow. Therefore, the problem: why the isolated turbulent band in pPF illustrates such a well-defined inclination angle, is thus still open.

The three-dimensional incompressible flow driven by a pressure gradient between two parallel walls is numerically simulated with a pseudo-spectral method [22], where 1.5 times of the bulk velocity U_m and the half channel height h are set as the characteristic velocity and length scales, respectively. No-slip boundary conditions are applied at the walls ($y = \pm 1$) and periodic boundary conditions are used in the streamwise (x) and spanwise (z) directions. The flow rate is kept constant and the flow field is expanded with Fourier modes (N_x and N_z) and Chebyshev polynomials (N_y) in the x , z , and y directions, respectively. The Reynolds number is defined as $Re = 1.5U_m h/\nu$, where ν is the kinematic viscosity of

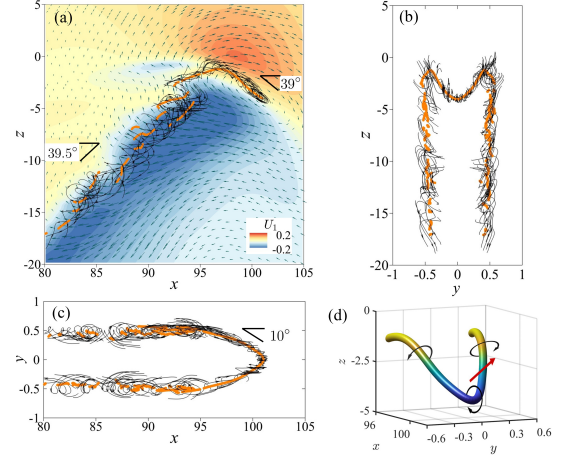


FIG. 1. Vortex cores (orange points) in the mean-flow modulation (\mathbf{U}_1) field of ITB obtained at $Re = 700$ in (a) the bottom view, (b) the front view, and (c) the side view, where the streamlines (black curves) are truncated to avoid cloaking the cores. U_1 and (U_1, W_1) fields at the midplane are shown by contours and vectors in (a), respectively. (d) The vortex cores in the downstream head are linked into a ν -shape vortex curve colored with z coordinate, whose nearby induced velocity and self-induced velocity are illustrated with the black and red arrows, respectively.

fluid, and it is checked that the computational domain of $(L_x \times L_y \times L_z) = (200 \times 2 \times 160)$ is large enough and the resolution of $(N_x \times N_y \times N_z) = (1024 \times 65 \times 1024)$ with a time step of 0.02 is fine enough to simulate the dynamic behaviors of ITB [5, 6].

As shown in Fig. 1(a), there is a high streamwise velocity region at the ITB head [7, 10], and hence the point with the maximum streamwise velocity at the midplane is named as head point and is tracked in the simulations to calculate its convection velocity $\mathbf{u}_H = (u_H, w_H)$, which is referred as the head convection velocity hereafter. The velocity of ITB is decomposed into three parts within a frame moving with \mathbf{u}_H , i.e., $\mathbf{U} = \mathbf{U}_0 + \mathbf{U}_1 + \mathbf{u}'$, where \mathbf{U}_0 , $\mathbf{U}_1 = (U_1, V_1, W_1)$, and \mathbf{u}' are the velocities of the basic flow, the mean flow modulation, and the perturbations, respectively. At $Re = 700$, the

* jjtao@pku.edu.cn

mean values of (u_H, w_H) are calculated as $(0.8667, 0.0994)$ with a convection angle $\theta_H = \arctan(w_H/u_H) = 6.54^\circ$, and \mathbf{U}_1 is obtained by averaging 13,900 fields with a time interval of 0.02 as shown in Fig. 1, where the traveling streaks are filtered out. Vortex cores, where $\nabla \mathbf{U}_1$ owns one real and a pair of complex-conjugate eigenvalues [23], are calculated and linked into a bent smooth curve at the ITB head [Fig. 1(d)], which is named as ν -shape vortex hereafter. It extends into the bulk part, forming a pair of counter-rotating vortex-tube type structures or vortex tube pair near $y = \pm 0.47$ as illustrated by the vortex cores in Fig. 1(a)-1(c). These large scale vortex structures make up the backbone of ITB. Note that in the frame co-moving with the ITB head, the upstream tail extends obliquely with time and the mean flow near the tail is too weak to calculate the vortex core.

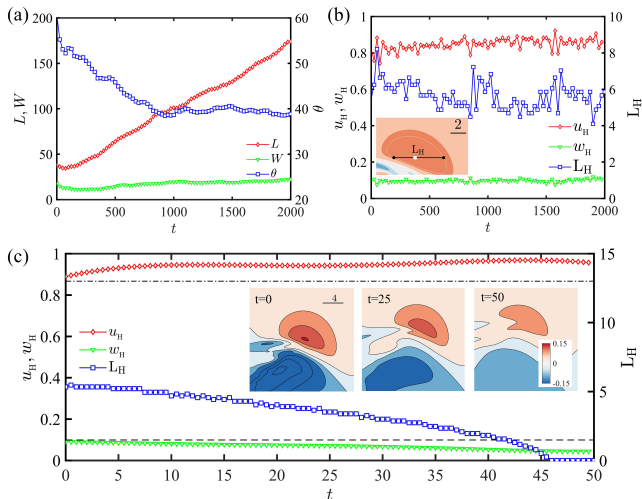


FIG. 2. (a) Geometric and (b) kinematic characteristics of the Oseen-type vortex initial disturbance measured every 1250 time steps during its evolution at $Re = 700$. Inset of (b): the white point denotes the head point and L_H is the length of the line segment where $U - U_0 \geq 0.8(U - U_0)_{max}$ ($t = 0$) at the midplane. (c) u_H and L_H during the decay of the mean-flow structure shown in Fig. (1). As references, (u_H, w_H) of ITB are shown by the dash dot and dashed lines, respectively. Inset of (c): the iso-contours of $U - U_0$ around the downstream head at the midplane.

The ν -shape vortex has two important effects. The first is the induced flow at its neighborhood, e.g., the high speed region labeled by the red contours in Fig. 1(a). The second is related to its curvature: similar to a vortex ring, the ν -shape vortex should have an obliquely forward self-induced velocity as illustrated by the red arrow in Fig. 1(d). In order to verify this conjecture and inspired by the vortex structures shown in Fig. 1, a wall-normal Oseen-type vortex superimposed with random noise is introduced as the initial disturbance,

$$\begin{cases} u'_\theta &= f(y) \frac{\Gamma}{2\pi r} \left[1 - \exp\left(-\frac{r^2}{R^2}\right) \right], \quad v' = 0 \\ f(y) &= \tanh\left(\frac{1+y}{\kappa}\right) + \tanh\left(\frac{1-y}{\kappa}\right) - 1, \end{cases} \quad (1)$$

where u'_θ is the azimuthal velocity normal to the y -direction vortex axis and r is the distance from the axis. The function $f(y)$ is used to damp the disturbance smoothly near the sidewalls, and the parameters (Γ, R, κ) are set as $(8, 2\sqrt{3}, 0.1)$ at $Re = 700$ in order to mimic the mean flow around the ν -shape vortex at the midplane. This initial disturbance first evolves to a local structure similar as the ITB head at about $t = 150$, and then extends obliquely by producing quasi-periodic streaks to form the bulk part. The length L , width W , and inclination angle θ with respect to the x direction of this evolving structure are calculated based on the centered second moments of disturbance kinetic energy relative to the basic flow, and for details of the calculation method we refer to the previous paper [6].

It is shown in Fig. 2(a) that both θ and W become statistically constant as $t > 1000$, indicating that a mature ITB is developed. During the extension process, e.g., $t = (150, 2000)$ when L increases from about 35 to 175 and θ decreases from about 53° to 40° , the segment length L_H shown in Fig. 2(b), which represents the perturbation strength and length scale of the ITB head, fluctuates with time but around a constant value, and (u_H, w_H) remain statistically constant, suggesting that the head structure and convection velocities are independent of the characters of the bulk part, e.g., the band length and the inclination angle. Specifically, when traveling streaks are filtered out, it is shown in Fig. 2(c) that the large-scale mean flow continues to move downstream for some time, when both u_H and w_H still retain values close to those of the ITB, denoting that the head convection velocity is intrinsically determined by the mean flow, not by the perturbations, e.g., the traveling streaks. Note that without the Reynolds stress contributed by the perturbation components, the mean-flow modulation field decays due to the viscous diffusion and dissipation as illustrated in the insets of Fig. 2(c), and the high speed region at the downstream head shrinks as illustrated by the L_H curve.

A natural question is what determines the convection velocity of the ITB bulk. In order to answer this question, a long and tilted computational domain [14] is used to simulate the bulk part as shown in Fig. 3(a), which has no head and tail and is referred as the bulk turbulent band (BTB) hereafter. Note that by rotating the coordinates about the x -axis, an ITB with an inclination angle θ can convert to a counterpart with $-\theta$, and hence only positive tilted angles of the computational domain θ_{CD} are considered, i.e., $0 < \theta_{CD} < 90^\circ$. Periodic boundary conditions are applied in both the longitudinal (Z) and the transverse (X) directions of the band. The computational domain has the same width $L_Z = 10$ as the previous study [11] but a longer length ($L_X = 200$) to reduce the band interaction brought by the periodic boundary condition applied in the X direction. Simulations are carried out with a resolution of $(N_X \times N_Y \times N_Z) = (1024 \times 64 \times 64)$, which is checked to be fine enough to simulate the properties of BTB.

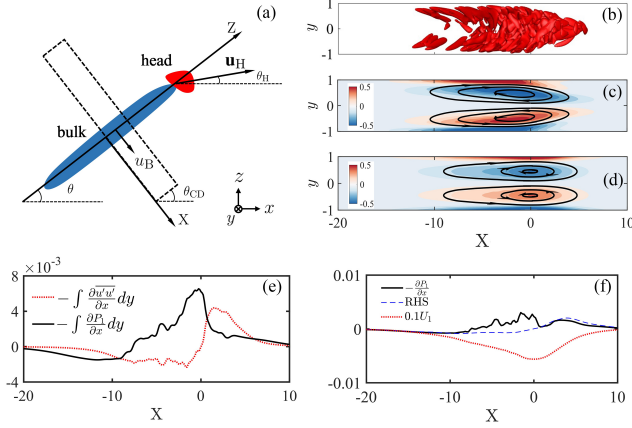


FIG. 3. Flow properties of BTB obtained at $Re = 700$. (a) Bottom view of the tilted computational domain labeled with dashed lines in the tilted $X - Z$ coordinates. (b) Iso-surface of the vortex criterion $Q = 0.02$ for transient perturbation field \mathbf{u}' . Iso-contours of Z -direction vorticity for the mean-flow modulation \mathbf{U}_1 obtained in simulations (c) and with the kinematic modal [Eq. (2)] (d). The black streamlines illustrate the vortex tube pair. (e) Integrals of pressure gradient and Reynolds stress in Eq. (3). (f) Pressure term and the total right hand side (RHS) of Eq. (5). In (c)-(f), the minimal U_1 at the midplane lies at $X = 0$.

The coordinate of BTB center X_c^B is defined with the normal disturbance velocity $V(X, y, Z, t)$ at the midplane as $X_c^B = \int_0^{L_x} \langle e_V \rangle_Z X dX / \int_0^{L_x} \langle e_V \rangle_Z dX$, where $\langle e_V \rangle_Z = \frac{1}{2L_z} \int_0^{L_z} V^2 dZ$, and then we can calculate the convection velocity of BTB, $u_B = dX_c^B/dt$. The same velocity decomposition as that of ITB is applied within a frame moving with u_B . It is noted that in the present configuration and parameter space, BTB can retain a saturated state with a constant u_B and a steady \mathbf{U}_1 field for at least 3000 time units. At $Re = 700$, \mathbf{U}_1 is obtained by averaging 20,000 fields with a time interval of 0.02, and the vortex structures of \mathbf{u}' and \mathbf{U}_1 are shown in Fig. 3(b) and 3(c), respectively. The streamlines in Fig. 3(c) illustrate clearly the vortex tube pair, which looks similar to the vortex dipole found in the mean flow of localized wave packet in two dimensional channel flows [24] but with reverse rotating directions.

Considering kinematic conditions for the mean flow: (a) no variation exists in the Z direction and hence $\partial U_1 / \partial X + \partial V_1 / \partial y = 0$, (b) no-slip conditions at the walls, (c) \mathbf{U}_1 is symmetric about the midplane, (d) the cross-section flow rate of \mathbf{U}_1 is zero, and (e) $U_1(y=0) = U_1^c$, (U_1, V_1) may be modeled with polynomials (u_1, v_1) as

$$u_1 = U_1^c(1 - 6y^2 + 5y^4), \quad v_1 = -\frac{dU_1^c}{dX}(y - 2y^3 + y^5). \quad (2)$$

It is shown in Fig. 3(d) that this kinematic model grasps the main features of the vortex tube pair shown in Fig. 3(c), e.g., the vorticity directions. The vortex centers predicted by the model lie at $y = \pm\sqrt{0.2} \simeq \pm 0.45$, which

are close to ± 0.47 , the simulation value for BTB.

Next, the momentum equations governing the mean flow are simplified in order to estimate u_B analytically. As shown in Fig. 3(c), the length scale of the vortex tube pair in the X direction is much larger than that in the y direction, and hence the pressure of the mean-flow modulation P_1 is nearly independent of y , or approximately $\partial P_1 / \partial X \simeq dP_1 / dX$. Integrating the time-averaged Navier-Stokes equation in the wall-normal direction and evaluating (U_1, V_1) with (u_1, v_1) , we have

$$\int_{-1}^1 \frac{\partial(P_1 + \overline{u'u'})}{\partial X} dy \simeq -\frac{256}{315} \frac{d(U_1^c)^2}{dX} - \frac{64}{105} \frac{dU_1^c}{dX} + \frac{16}{Re} U_1^c, \quad (3)$$

where the overline indicates the time average. Noticing that near the downstream end (e.g., $X > 5$) $\int_{-1}^1 \frac{\partial P_1}{\partial X} dy \simeq \int_{-1}^1 \frac{\partial \overline{u'u'}}{\partial X} dy$ [Fig. 3(e)], Eq. (3) is simplified as

$$\frac{\partial P_1}{\partial X} \simeq \frac{dP_1}{dX} \simeq -\frac{64}{315} \frac{\partial(U_1^c)^2}{\partial X} - \frac{16}{105} \frac{\partial U_1^c}{\partial X} + \frac{4}{Re} U_1^c. \quad (4)$$

At the midplane of the moving frame, the time-averaged X -direction momentum equation is

$$[\sin(\theta_{CD}) - u_B + U_1^c] \frac{\partial U_1^c}{\partial X} = -\frac{\partial P_1}{\partial X} + \frac{1}{Re} \nabla^2 U_1 + RS, \quad (5)$$

where RS represents the Reynolds stress term. It is shown in Fig. 3(b) that the small-scale perturbation vortex structures concentrate near the midplane at the downstream side of BTB, and then the corresponding Reynolds stress is localized in the y direction as well. In order to retain the mean flow modulation near the midplane, RS in Eq. (5) should be balanced mainly by the viscous diffusion term instead of the pressure gradient, which is almost uniform in the y direction. This conjecture is confirmed by the numerical data shown in Fig. 3(f), where the right hand side (RHS) of Eq. (5) nearly coincides with $-\partial P_1 / \partial X$ as $X > 1$, indicating that RS and the viscous diffusion term nearly cancel out each other near the downstream midplane. Consequently, u_B can be evaluated analytically after substituting Eq. (4) into Eq. (5) as

$$u_B \simeq \sin(\theta_{CD}) - \frac{16}{105} + \frac{187}{315} U_1^c + \frac{4U_1^c}{Re} \frac{\partial U_1^c}{\partial X} \simeq \sin(\theta_{CD}) - \frac{16}{105}. \quad (6)$$

Note that at the downstream midplane of BTB as shown in Fig. 3(f), $|U_1^c| \ll 1$, $\frac{\partial U_1^c}{\partial X} > 0$, and $|\frac{U_1^c}{Re} \frac{\partial U_1^c}{\partial X}| \ll 1$ due to $Re \gg 1$. At $Re = 700$ and $\theta_{CD} = 40^\circ$, Eq. (6) predicts that $u_B \simeq 0.49$, which agrees well with the simulation value 0.48, indicating that the present dynamic analyses grasp the key feature of the mean-flow structure. According to vorticity kinematics, the rotating directions of the vortex tube pair shown in Fig. 3(c) correspond to a backward self-induced velocity, which may be estimated by deducting the basic flow velocity

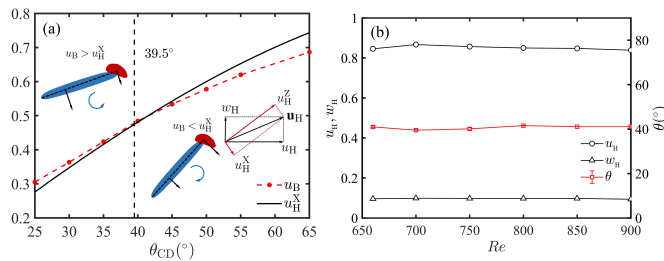


FIG. 4. (a) Convection velocity of BTB (u_B) and the projection of the head convection velocity in the X direction u_H^X obtained numerically at $Re = 700$ and different domain angles θ_{CD} . (b) Head convection velocity and inclination angle of ITB as functions of Re .

at the vortex center from u_B and the same value -0.02 is obtained for both the model and the simulations.

By comparing u_B obtained numerically at different θ_{CD} and $u_H^X = |\mathbf{u}_H| \sin(\theta_{CD} - \theta_H)$, the projection of ITB's head convection velocity in the X direction, an angle selection mechanism of ITB is proposed. It is shown in Fig. 4(a) that when $\theta < 39.5^\circ$, the corresponding u_B is larger than u_H^X , and this velocity difference exerts an angular momentum to rotate anticlockwise the ITB during its movement, increasing the inclination angle θ ; while for $\theta > 40.5^\circ$, $u_B < u_H^X$ and hence the ITB will rotate clockwise, leading to the decrease of θ . Therefore, the selection of ITB's inclination angle $\theta \simeq 40^\circ$ is a result of competition between u_B and u_H^X through a self-adjustment process. In fact, this process has been illustrated in Fig. 2(a), where the inclination angle of the vortex-triggered band structure decreases with time

until it reaches the equilibrium value around $t = 1000$.

According to Eq. (6), the bulk convection velocity is mainly determined by the large-scale mean flow and is a weak function of Re , so is the head convection velocity shown in Fig. 4(b). Consequently, the inclination angle of ITB is basically independent of Re as well due to the self-adjustment mechanism and retains around 40° [Fig. 4(b)], a value consistent with the experimental measurements [10]. When turbulent bands interact with each other, e.g., the parallel arranged turbulent bands observed at high Reynolds numbers [25], their inclination angles may be different from that of the ITB.

At low and moderate Reynolds numbers, the isolated turbulent band is the typical transitional structure of channel flows, and its most curious feature is probably the characteristic inclination angle of the bulk. Based on numerical simulations, kinematic modeling, and dynamic analyses, it is shown that the inclination angle is not determined by the bulk part itself, but by a balance between the convection velocities of the bulk and the downstream head: the difference between these convection velocities exerts an angular momentum to rotate the ITB until the specific inclination angle is achieved, indicating the crucial role played by the head part in the angle selection mechanism. This self-adjustment mechanism provides new insights into how localized turbulence behaves during the subcritical transitions in wall-bounded shear flows.

The simulations are performed on TianHe-1(A), and the help on SIMSON from P. Schlatter, L. Brandt, and D. Henningson is gratefully acknowledged. This work is supported by the National Natural Science Foundation of China (Grants Nos. 91752203).

-
- [1] L. S. Tuckerman, M. Chantry, and D. Barkley, *Annu. Rev. Fluid Mech.* (2020).
 - [2] M. Avila, D. Barkley, and B. Hof, *Annu. Rev. Fluid Mech.* **55**, 575 (2023).
 - [3] X. Wu, *Annu. Rev. Fluid Mech.* **55** (2023).
 - [4] J. Tao and X. Xiong, in *14th Asian Congress of Fluid Mechanics* (Hanoi and Halong, Vietnam, 2013).
 - [5] X. Xiong, J. Tao, S. Chen, and L. Brandt, *Phys. Fluids* **27**, 41702 (2015).
 - [6] J. J. Tao, B. Eckhardt, and X. M. Xiong, *Phys. Rev. Fluids* **3**, 011902(R) (2018).
 - [7] Kanazawa, Ph.D. thesis, Osaka University (2018).
 - [8] M. Shimizu and P. Manneville, *Phys. Rev. Fluids* **4**, 113903 (2019).
 - [9] X. Xiao and B. Song, *J. Fluid Mech.* **883** (2020).
 - [10] J. Liu, Y. Xiao, L. Zhang, M. Li, J. Tao, and S. Xu, *Phys. Fluids* **32**, 121703 (2020).
 - [11] C. S. Paranjape, Y. Duguet, and B. Hof, *J. Fluid Mech.* **897** (2020).
 - [12] V. Mukund, C. Paranjape, M. P. Sitte, and B. Hof, *arXiv preprint arXiv:2112.06537* (2021).
 - [13] Y. Duguet and P. Schlatter, *Phys. Rev. Lett.* **110**, 034502 (2013).
 - [14] L. S. Tuckerman, T. Kreilos, H. Schrobdsdorff, T. M. Schneider, and J. F. Gibson, *Phys. Fluids* **26**, 114103 (2014).
 - [15] S. Gomé, L. S. Tuckerman, and D. Barkley, *Phys. Rev. Fluids* (2020).
 - [16] G. Kawahara, M. Uhlmann, and L. van Veen, *Annu. Rev. Fluid Mech.* **44**, 203 (2012).
 - [17] M. Nagata, *J. Fluid Mech.* **217**, 519 (1990).
 - [18] F. Reetz, T. Kreilos, and T. M. Schneider, *Nature communications* **10**, 2277 (2019).
 - [19] P. Manneville, *Fluid Dyn. Res.* **43**, 065501 (2011).
 - [20] P. Manneville, *EPL* **98**, 64001 (2012).
 - [21] P. V. Kashyap, Y. Duguet, and O. Dauchot, *Phys. Rev. Lett.* **129**, 244501 (2022).
 - [22] M. Chevalier, P. Schlatter, A. Lundbladh, and D. S. Henningson, *Tech. Rep. TRITA-MEK 2007:07* (KTH Mechanics, 2007).
 - [23] D. Sujudi and R. Haimes, in *12th Computational fluid dynamics conference* (1995) p. 1715.
 - [24] Y. Xiao, J. Tao, and L. Zhang, *Phys. Fluids* **33**, 031706 (2021).
 - [25] T. Tsukahara, Y. Kawaguchi, and H. Kawamura, *arXiv preprint arXiv:1406.1378* (2014).